2012

Shallow Flow Past a Cavity: Effect of Gravity Wave Coupling

Maxwell Marshall Wolfinger
Lehigh University

SHALLOW FLOW PAST A CAVITY: EFFECT OF GRAVITY WAVE COUPLING

by

Maxwell Wolfinger

A Thesis

Presented to the Graduate and Research Committee

of Lehigh University

in Candidacy for the Degree of

Master of Science

in

Mechanical Engineering

Lehigh University

May 2012

This thesis is accepted and approved in partial fulfillment of the requirements for the Master of Science.

_____
Date

_____
Professor Donald Rockwell

_____
Professor Gary Harlow

TABLE OF CONTENTS

Title……..i

Certificate of Approval…….……ii

Table of Contents……..……iii

List of Figures……iv

Abstract…….……..1

1. Introduction……..……...…….2

2. Experimental Systems and Techniques…….……...6

3. Pressure Measurements…….11

4. Imaging of Flow Structure……..…..13

4.1 Time Averaged Patterns…….……14

4.2 Phase Averaged Patterns……..……..17

5. Conclusions……19

References……22

Appendix……..25

Vita……..42

LIST OF FIGURES

Figure 1a: Schematic of water channel test section and insert for investigation of shallow flow……26

Figure 1b: Schematic of experimental test section including quantitative imaging system, undulating sheer layer along mouth of cavity, and unsteady detection of the surface due to resonant mode of gravity wave within the cavity……..27

Figure 2: Spectral response of pressure fluctuation at the impingement corner of cavity as a function of dimensionless velocity of inflow……..28

Figure 3: Frequency of peak spectral response of pressure fluctuation at the impingement corner as a function of inflow velocity……..…29

Figure 4: Amplitude of spectral peak of fluctuating pressure at two locations as a function of inflow velocity……30

Figure 5: Contours of constant root-mean-square of cross stream velocity as a function of inflow velocity. …….31

Figure 6: Spectral response of cross-stream velocity fluctuation along the shear layer of a shallow cavity (variable x/L along y/L =0) in absence of gravity-wave coupling (U_{av}/f_nL = 0.78; left image) and with coupling. (U_{av}/f_nL = 1.44; right image)……...……32

Figure 7: Contours of constant Reynolds Stress as a function of inflow velocity.....32

Figure 8: Contours of constant time-averaged cross stream velocity as a function of inflow velocity……..33

Figure 9: Contours of constant time-averaged vorticity as a function of inflow velocity……..34

Figure 10: Contours of constant phase-averaged vorticity at 40° intervals for dimensionless velocity U_{av}/f_nL = 1.44, corresponding to coupling of shear layer instability along the opening of cavity and a streamwise-oriented gravity wave within the cavity…….35

Figure 11: Contours of constant phase-averaged cross-stream velocity at 40° intervals for dimensionless velocity U/f_oL = 1.44, corresponding to coupling of shear layer instability along the opening of cavity and a streamwise-oriented gravity wave within the cavity…36

Figure A1: Isometric view of water channel test section and insert……..37

Figure A2: Contours of constant Reynolds Stress at 40° intervals for dimensionless velocity U/f_nL = 1.44, corresponding to coupling of shear layer instability along the opening of cavity and a streamwise-oriented gravity wave within the cavity……38

Figure A3: Contours of constant root mean square of cross-stream velocity at 40° intervals for dimensionless velocity U/f_nL = 1.44, corresponding to coupling of shear layer instability along the opening of cavity and a streamwise-oriented gravity wave within the cavity…….….39

Figure A4: Frequency of peak spectral response of pressure fluctuation at the impingement corner as a function of inflow velocity, including those not representing the primary gravity wave resonance…….40

Figure A5: Frequency of peak spectral response of pressure fluctuation inside the cavity as a function of inflow velocity including those not representing the primary gravity wave resonance…….41

ABSTRACT

Shallow, fully turbulent inflow past a cavity can give rise to highly organized oscillations, due to coupling between: (i) the inherent instability of the separated turbulent layer along the opening of the cavity; and (ii) a gravity standing wave within the cavity. Techniques of particle image velocimetry and pressure measurements are employed to characterize the occurrence of the fully-coupled state of the oscillation, relative to its uncoupled state. At a threshold value of inflow velocity, the frequency of the inherent instability of the turbulent separated shear layer locks-on to the frequency of the gravity standing wave. Moreover, the amplitude of the spectral peak of the pressure fluctuation, both at the impingement corner of the cavity and within the cavity, attains maximum values when lock-on occurs.

Occurrence of a fully coupled or locked-on state substantially alters the time-averaged flow structure. Enhanced magnitudes of patterns of Reynolds stress and transverse velocity fluctuation occur along the cavity shear layer. Simultaneously, increased flow from within the cavity towards the separated shear layer occurs at a location immediately downstream of separation at the leading-edge of the cavity and, correspondingly, increased flow into the cavity occurs in the impingement region. The influence of the locked-on state is therefore global: both the separated shear layer along the mouth of the cavity and the flow within the cavity are substantially altered.

Phase-averaged representations of the flow structure show highly coherent, phase-locked patterns of vorticity along the cavity opening during the locked-on state. These vorticity patterns are associated with large, phase-locked excursions of the transverse component of velocity, within both the separated the shear layer and the cavity.

1. INTRODUCTION

Shallow flows can occur in the form of rivers, lakes, bays, and estuaries. In such flows, the bottom surface is a solid bed, while the upper surface is an essentially a shear-free (water-air) interface, and both the length and width of the flow are much larger than its depth h_w. Furthermore, the wavelength of an instability λ or the characteristic diameter D of a large-scale vortex formed in a shallow flow are much larger than the water depth h_w, i.e. $\lambda / h_w >> 1$ and $D / h_w >> 1$. Shallow flows are typically turbulent, and the streamwise length L from their origin is sufficiently long compared to the water depth, $L / h_w > 50$, that the turbulence between the free surface and the bed is considered to be fully-developed. This small-scale three-dimensional turbulence, however, has a length scale ℓ that is of the order or less than the water depth, i.e., $\ell / h_w < 1$. Although there is a degree of interaction between the aforementioned large and small-scales, the onset and development of the large-scale instability and vortex formation are considered as quasi-two-dimensional phenomena. (Jirka and Uijttewaal, 2004)

A shallow flow may contain various obstacles, merging streams and other geometrical variations that lead to formation of basic classes of shear flows in the horizontal plane. The existence of an instability leading to vortex formation in shallow jets, mixing-layers and wakes of infinite streamwise extent is determined by the dimensionless stability parameter S, which can be represented by $S = \bar{c}_f \delta \overline{U} / 2h\Delta U$ where $\bar{c}_f$ is the bed friction coefficient, δ is the width of the transverse shear flow, $\overline{U}$ represents the average velocity across the shear layer, ΔU is the corresponding velocity difference across the layer, and h is the water depth. (Chu and Babarutsi, 1988) The

velocity difference ΔU exerts a destabilizing influence on the onset of the instability, whereas the friction coefficient $\overline{c_f}$ (in the range of 0.005 to 0.01 for laboratory and field conditions) promotes stabilization. A self-excited instability leading to vortex formation can therefore occur only when the value of the bed friction number S is sufficiently small.

Instability and vortex formation in shallow mixing layers, jets and wakes of infinite streamwise extent. Laboratory investigations, as well as analyses and numerical simulations, have focused on shallow separated shear flows of large (essentially infinite) streamwise extent, and substantial advances in our understanding have been achieved in recent decades. Representative works on instabilities and vortex formation in basic categories of shear flows include the shallow jet (Giger et al., 1991; Dracos et al, 1992; Jirka, 1994; and Chen and Jirka, 1998), shallow wake (Ingram and Chu, 1987; and Chen and Jirka, 1995 and 1997), and the shallow mixing layer (Chu and Babarutsi 1988; Chen and Jirka, 1997; and van Prooijen and Uijttewaal, 2002). Analyses/simulations of the foregoing classes of shallow separated shear flows based on linear stability theory have been undertaken by a number of investigators. Representative studies include those of Chu et al. (1991), Chen and Jirka (1997), van Prooijen and Uijtewaal (2002), Kolyshkin and Ghidaoui (2003), Socolofsky and Jirka (2004), and Chan et al. (2006). The criteria for existence of convective and absolute instabilities in shallow shear layers, and their consequences for large-scale vortex formation, have been established.

Instability and vortex formation in shallow mixing layers of finite length. In contrast to shallow mixing layers of infinite length, shallow mixing layers having a finite length scale (in the streamwise direction) have received relatively little attention. Investigations of shallow mixing layers with finite streamwise length have primarily involved flow past cavity configurations. The experimental works of Weitbrecht and Jirka (2001), Uijttewaal et al. (2001) and Kurzke et al. (2002) and the computational studies of McCoy et al. (2008) provide valuable insight into flow patterns within the cavity and the associated purging of marker material.

The configuration of a rectangular cavity in shallow flow can be viewed as representative of a spur dyke or embayment, which are susceptible to resonant response in the form of a standing gravity wave or Helmholtz resonance. The instability arising in the separated, shallow layer along the opening of such a semi-enclosed geometry can potentially couple with a mode of the standing gravity wave, thereby giving rise to well-defined oscillations. Field measurements in Japan by Chen and Ikeda (1996), Ikeda et al. (1999) and Nezu and Onitsuka (2002) have revealed ordered undulations of the free-surface. The manner in which the gravity wave resonance can be instigated, and potentially couple with the instability/vortex formation along the separated shear layer, was not addressed. Such coupling may strongly influence the mass exchange and purging processes form the cavity to the main stream (river).

Small-scale laboratory experiments were performed by Kimura and Hosoda (1997), who employed qualitative visualization of the large-scale vortical structures along the opening of a rectangular cavity, and carried out computations to determine the velocity vectors along and within the cavity. Furthermore, they determined experimentally that a

longitudinal (streamwise- oriented) gravity standing wave existed within the cavity, and it influenced the aforementioned vortical structures. Ekmekci and Rockwell (2007) examined vortex formation in presence of shallow (free-surface) oscillations for a cavity geometry that was the equivalent of the classical organ pipe. The degree of coherence of the vortical structures was a function of the degree of coupling between the shear layer instability and a standing wave mode within the organ pipe-like cavity.

Unresolved issues. The preceding investigations have provided insight into various aspects of shallow flow instabilities, including those with finite streamwise length scale. Considering the focus of the present investigation, the major unclarified points are as follows:

Shallow flow past a rectangular cavity represents a generic configuration applicable to a range of river and coastal flows. The potential exists for coupling between the inherent instability of the shallow, separated shear layer along the opening of the cavity and a standing gravity wave mode within the cavity. The conditions associated with possible lock-on, namely control of the instability/vortex formation frequency of the separated shear layer by the eigenfrequency of the gravity wave mode within the cavity, have not been characterized. Moreover possible occurrence of a peak amplitude response of the coupled shear layer-cavity mode with variation of the inflow velocity has not been addressed.

For the case of a fully-developed turbulent flow in the shallow layer approaching the rectangular cavity, highly coherent vortex formation in the separated shear layer along

the cavity may occur. The onset of coupling between the nominally turbulent shear layer and a gravity wave mode of the cavity may lead to the development of highly coherent, phase-locked vortex formation, but this concept has not been explored.

If lock-on, i.e. strong coupling, exists between the inherent instability of the separated shear layer along the cavity and a gravity standing mode within the cavity, modification of the separated shear layer relative to its non- locked-on state may yield substantial changes in the time-averaged turbulence statistics of the separated shear layer, that is, Reynolds shear and normal stresses. Potential enhancement of flow patterns that represent the flow statistics should be addressed.

In the event that substantial modification the separated shear layer occurs in the presence of lock-on, the manner in which the flow within the cavity is modified has not been assessed. For example, increased Reynolds stress in the separated shear layer will be associated with enhanced entrainment demands of the layer, and potentially a change in the flow drawn from the cavity towards the separated layer. This concept deserves attention.

2. EXPERIMENTAL SYSTEM AND TECHNIQUES

Experiments were conducted in a large, free surface water channel. The test section of this channel had an overall length of 4,877 mm, a width of 927 mm, and a water depth adjustable up to 610 mm. Figures 1a and 1b show details of the test section and a specially designed insert, which is located within the test section, in order to allow characterization of shallow flow past a cavity. This insert is designed to optimize insight into the separated shear layer along the mouth of the cavity, in relation to the flow pattern

within the cavity, while accounting for varying degrees of coupling between the separated layer and a gravity standing wave within the cavity. The test section insert consists of a 12.7 mm thick acrylic (transparent) plate which is elevated a distance of 165 mm above the floor (bottom surface) of the test section. The streamwise length of the shallow layer, from the leading edge of the horizontal acrylic plate to the leading (upstream) corner of the cavity is L_i = 1905 mm. The plan view of Figure 1a indicates (with gray shading) the contraction, which has a radius of curvature of 457 mm. The width and streamwise length of the channel located downstream of the contraction, are respectively W_e = 457 mm and L_e = 1384 mm. The cavity has a length of L = 305 mm, and the continuation of the channel, located downstream, has a length of L_o = 838 mm. All of these components have a height h_a = 102 mm, and are fabricated from acrylic. The height of the shallow water layer was maintained at a constant value of h_w = 38 mm over the range of depth averaged velocity U_{av} = 243 to 470 mm/s. This range of velocity U_{av} corresponds to the following values of Reynolds number: $\mathrm{Re}_{Li} = 4.62 \times 10^5$ to 8.92×10^5 based on depth averaged inflow velocity U_{av} and length L_i of the false floor upstream of the cavity; and Re_{hw} = 9,210 to 17,800 based on U_{av} and water depth h_w. The foregoing parameters correspond to a ratio of the inflow length to water depth of L_i / h_w = 50.1. According to the criterion of Uijttewaal et al. (2001), for a fully evolved turbulent shallow layer to be attained, $L_i / h_w > 50$. Boundary layer trips of 1.6 mm thickness and length of 13 mm were placed at the indicated positions on the bottom wall of the insert and the vertical surface of the inflow channel, at a location immediately downstream of the contraction. These trips insure rapid onset of a turbulent boundary layer and attainment of a fully turbulent layer along the floor (bottom surface) of the insert as

verified by the horizontal velocity distribution adjacent to the acrylic boundary, which corresponded to a 1/7 power law distribution at a location 26 mm upstream of the leading-corner of the cavity. Furthermore, away from the vertical leading-edge of the cavity (x = -26 mm and y = 52 mm), the velocity distribution in the vertical direction is also represented well by same type of power law distribution.

Figure 1b shows detailed plan views of the cavity configuration, including the separated shear layer along the mouth of the cavity. The side view of Figure 1b illustrates the unsteady deflection of the free surface within the cavity, which is due to coupling between the inherent instability of the separated layer along the mouth of the cavity and the n = 1 mode of gravity wave resonance within the cavity. During preliminary experiments, the parameters W, L and h_w were varied in order to determine the configuration which produced a well-defined gravity wave resonance within the cavity. These values are L = 305 mm, W = 457 mm, and h_w = 38 mm, over the range of depth averaged velocity U_{av} which extended from 243 to 470 mm/s. A well defined gravity standing wave of peak amplitude h_d = 2 mm, as defined in Figure 1b, can be attained, corresponding to coincidence of the inherent instability frequency of the shear layer along the mouth the cavity and the eigenfrequency of the gravity wave mode. This peak amplitude corresponds to a ratio of the wave amplitude h_d to the water depth h_w of h_d / h_w = 0.05.

Prediction of the eigenfrequency of the first eigenmode of the gravity standing wave, which is aligned in the streamwise direction x (see Figure 1b), and uniform along the depth of the cavity, is described by Kimura and Hosoda (1997) and Naudascher and Rockwell (1994). The equation for the eigenfrequencies is:

$$f = \frac{n\sqrt{gh}}{2L} \quad n = 1, 2, 3 \ldots \quad (1)$$

in which L is the cavity length, g is acceleration due to gravity, h_w is the water depth, and n and f are the mode and frequency of oscillation. The first mode of the standing gravity wave corresponds to n = 1, for which the wavelength of the standing gravity wave is twice the length of the cavity. This mode is represented by the schematic of Figure 1b. The predicted frequency according to equation (1) is 1.0 Hz, which compares to the experimentally determined value of 1.02 Hz.

The amplitude and frequency of the coupled shear layer-standing wave oscillation was characterized at the impingement (downstream) corner of the cavity, as well as within the cavity, over the range of inflow velocities. This was accomplished using two pressure transducers, at the locations defined in Figure 1b. The first of these transducers, designated as P_a, is located at the corner of the cavity. The second transducer, designated as P_b, is located a horizontal distance of 229 mm within the cavity, measured from its corner. Both transducers P_a and P_b are located at an elevation of h_p = 13 mm from the bottom surface, i.e., at z = 13 mm, where z is defined in Figure 1b. The peak oscillation amplitude occurred at a value of depth-averaged inflow velocity of U_r = 447 mm/s. In order to examine the onset and attenuation of the free surface oscillation, the flow structure along the cavity mouth was examined in detail at values of U_{av}/U_r = 0.54, 0.78, 1.0 and 1.05. These inflow velocities corresponded to values of momentum thickness θ/L on the vertical wall (at a location x/L =-0.1) from .016 to .020, and values of Reynolds number based on θ of 1,506 = Re_θ = 2,304. The Froude number, based on depth averaged inflow velocity and water depth had values extending over the range 0.40 = Fr

$=U_{av}/(gh_w)^{1/2}$ = 0.77 and the value of the bed friction number had values of 1.6x10^-3 = S = 1.9x10^-3 at separation and from 2.0x10^-3 = S = 3.0x10^-3 at x/L = 0.5.

The pressures at locations P_a and P_b designated in Figure 1b were measured with a PCB model 106B50 piezoelectric pressure transducer with a 480E09 signal conditioner. These signals were recorded using National Instruments LabView. The sampling rate was 20 Hz over a record time of 51.2s, corresponding to a total of 1024 samples. Ten of these time records were acquired for each inflow velocity. These results were then transformed into the frequency domain and averaged.

The quantitative structure of flow patterns at the indicated inflow velocities was determined with digital particle image velocimetry (DPIV). The flow was seeded with 12 μm diameter, metallic coated, hollow, plastic spheres which were illuminated with a double pulsed Nd:YAG laser, as represented in Figure 1b. This laser had a maximum output of 90mJ. The height of the laser sheet above the bottom surface was $z_L = h_L$ = 19 mm which corresponded to one half the depth h_w of the water. The delay time between laser pulses was varied between 2 and 3 ms for different inflow velocities, in order to minimize the number of spurious vectors produced during image processing. The laser pulse repetition rate was 15 Hz such that 15 image pairs could be acquired per second. A digital camera using a charge-coupled device (CCD) sensor was used to image the illuminated particles; it was synchronized with the laser system. This camera was placed below the water channel as shown in Figure 1b, and oriented orthogonal to both the streamwise (x) and cross-stream (y) directions. The camera sensor was a 1,600 pixel x 1,200 pixel element, and the effective magnification was 4.27 pixels/mm. Evaluation of image pairs was accomplished using a cross correlation technique with 32 x 32 pixel

interrogation windows and an effective overlap of 50%. This resulted in a vector field of 7,227 vectors in the x and y directions corresponding to an effective grid size of 3.66 mm. These vectors were then validated using local averages and replaced if they were found to be spurious. The total number of spurious results for this evaluation technique was less than 1% of all vectors.

The time-averaged flow structure and turbulence statistics were determined for the four inflow velocities U_{av}/U_r = 0.54, 0.78, 1.0 and 1.05. A total of 1,600 instantaneous images were acquired at each value of U_{av}/U_r. Phase-averaging of instantaneous images was performed at the dimensionless velocity U_{av}/U_r = 1 corresponding to resonant coupling between the instability of the separated layer along the mouth the cavity and the gravity standing wave within the cavity. This phase-averaging was accomplished by sampling the signal from the pressure transducer P_b located within the cavity during acquisition of instantaneous images, and using this measurement as reference to sort the vector fields into phase windows. The phase window (bin) size for this sorting was 10 degrees. This led to a minimum of 60 images per phase window. These 60 images were then used to compute the phase-averaged flow structure and turbulence statistics for each window.

3. PRESSURE MEASUREMENTS

The degree of coupling between the separated shear layer along the opening (mouth) of the cavity and the gravity standing wave within the cavity was assessed via pressure measurements at the locations P_a and P_b designated in Figure 1b. Pressure P_a indicates contributions from both the unsteady shear layer and the gravity wave at the impingement

corner, while pressure P_b represents only the contribution of the gravity standing wave during the coupled oscillation. Spectra of these pressure fluctuations were acquired over the range of increasing inflow velocity that included the onset of the fully-coupled resonant (locked-on) oscillation, followed by its attenuation. The inflow velocity is represented by the dimensionless ratio U_{av}/f_nL, in which U_{av} is the depth-averaged velocity, f_n is the frequency of the gravity standing wave (first mode), and L is the streamwise length of the cavity.

Figure 2 shows an isometric view of the pressure spectra $S_p(f)/1/2\rho U_{av}^2$ at seven representative values of inflow velocity U_{av}/f_nL. At low inflow velocities, spectra are low amplitude and ill defined. For values of $U_{av}/f_nL > 1.0$ a distinct peak is evident at $f/f_n = 1$. In addition, the first harmonic of this primary peak, due to nonlinear effects, is evident at $f/f_n = 2$. Increase of U_{av}/f_nL over the range 1.13 to 1.44 yields successive increases in the magnitudes of both the primary spectral peak at $f/f_n = 1$ and its first harmonic at $f/f_n = 2$. For higher values of $U_{av}/f_nL = 1.52$ and 1.57, the magnitudes of both of these peaks decrease.

Figure 3 shows the dimensionless frequency f_o/f_n as a function of the dimensionless inflow velocity U_{av}/f_nL for the pressure fluctuation p_a at the impingement corner. Frequency f_o is the frequency corresponding to the spectral peak of the fluctuation, which is represented by P_a in Figure 2, and f_n is the frequency of the gravity standing wave within the cavity. At low values of inflow velocity f_o/f_n varies linearly with U/f_nL. At a value of $U_{av}/f_nL = 1.2$, onset of the region of lock-on occurs, represented by $f_o/f_n = 1.0$. This region of lock-on extends up to $U_{av}/f_nL = 1.75$; within this region, the value of f_o remains within 5% of f_n. It is evident, by comparison with Figure 2, that increasing, as

well as decreasing amplitudes of the spectral peak of P_a can occur within this lock-on region, that is, locked-on oscillations are attainable over a range of amplitudes of the coupled shear layer-gravity wave oscillation.

In Figure 4, the magnitude of the spectral peak, designated as $S_p(f)_{max}/(1/2\rho U_{av}^2)$, is plotted against U_{av}/f_nL for the pressure fluctuations P_a and P_b. Consider, first of all the variation of the pressure P_a at the impingement corner. This magnitude rapidly increases with U_{av}/f_nL, and attains a maximum at $U_{av}/f_nL = 1.4$. Further increase of U_{av}/f_nL yields a severe decrease in the magnitude of the spectral peak. The corresponding variation of the peak magnitude of the gravity standing wave within the cavity, represented by P_b, also attains a maximum value at $U_{av}/f_nL = 1.4$. For pressure P_b, however, the onset of a rapid rise in amplitude does not occur until $U_{av}/f_nL = 1.3$, i.e., onset of detectable gravity wave resonance is not evident at lower values of U_{av}/f_nL. This observation indicates that the initial rise of the amplitude of pressure P_a, which commences at $U_{av}/f_nL = 0.8$, is instigated by the inherent instability of the separated shear layer along the opening of the cavity, in absence of significant resonance of the gravity standing wave. The spectral peaks at P_b below $U_{av}/f_nL = 1.2$ are low level, on the order of one tenth the amplitude of the spectral peak at $U_{av}/f_nL = 1.4$, but they are well defined and occur near the resonant frequency of the cavity f_n.

4. IMAGING OF FLOW STRUCTURE

Using the aforementioned pressure measurements as a guide, representative flow velocities U_{av}/f_nL were selected for quantitative imaging. The aim is to clarify the flow structure for the following regimes: insignificant oscillation; onset of oscillation;

attainment of peak oscillation amplitude; and attenuation of the oscillation. These regimes represent varying degrees of coupling between the instability of the separated shear layer along the opening (mouth) of the cavity and the gravity standing wave within the cavity. These regimes correspond to U_{av}/f_nL = 0.78, 1.13, 1.44 and 1.51.

Evaluation of the flow structure based on the acquired images was accomplished in two ways. First, time-averaged patterns of velocity, velocity components, and vorticity, as well as turbulence statistics, were determined. In addition to these time-averaged representations, phase-averaged patterns were determined at the dimensionless flow velocity U_{av}/f_nL = 1.44, corresponding to the peak spectral amplitude of the pressure fluctuation. These phase-averaged patterns provide insight into the time evolution of the flow structure over an oscillation cycle.

4.1 Time-Averaged Patterns

Figure 5 shows patterns of root-mean-square transverse velocity v_{rms} normalized by the depth-averaged inflow velocity U_{av}, i.e., v_{rms} / U_{av}, as a function of dimensionless velocity U_{av}/f_nL. At the lowest value of U_{av}/f_nL = 0.78, the flow is well below its locked-on state, as evident in Figure 3 and, furthermore, the associated pressure fluctuations, described in Figure 4, are minimal. Correspondingly, the peak magnitude of v_{rms} / U_{av} at U_{av}/f_nL = 0.78 is relatively low. At successively larger values of U_{av}/f_nL = 1.13 and 1.44, the peak magnitude of v_{rms} / U_{av} successively increases, in accord with the approach to, and occurrence of, locked-on oscillations, evident by comparison with Figure 3. Moreover, U_{av}/f_nL = 1.44 represents the maximum attainable peak of the pressure spectrum, as shown in Figure. At U/f_nL = 1.51, the peak amplitude of v_{rms} / U_{av} has decreased relative to that at U_{av}/f_nL = 1.44, which is compatible with the decrease of the

magnitude of the spectral peak of pressure indicated in Figure 4. Taking an overview of all of the patterns of v_{rms} / U_{av} in Figure 5, it is evident that the occurrence of coupling between the separated shear layer along the opening of the cavity and the gravity standing wave can have a major influence on the magnitude of the transverse fluctuation of the shear layer. That is, at $U_{av}/f_nL = 1.44$, the magnitude of v_{rms} / U_{av} is approximately a factor of 1.5 larger than the magnitude at $U_{av}/f_nL = 0.78$, where insignificant coupling occurs.

Further insight into the distinction between cases of insignificant and complete coupling between the separated shear layer along the opening the cavity and the gravity standing wave is provided in Figure 6. Spectra of the velocity fluctuation along the shear layer are shown as a function of streamwise distance along the cavity opening. Each spectrum was determined from the time history of the velocity signal, as extracted from the cinema sequence of quantitative images. A total of eight spectra were averaged at each of the ten streamwise locations along the cavity opening. These velocity spectra are shown at two extreme values of dimensionless velocity: $U_{av}/f_nL = 0.78$ and $U_{av}/f_nL = 1.44$, corresponding respectively to conditions well before and at occurrence of complete coupling between the separated shear layer along the cavity opening and the standing gravity wave within the cavity. The spectra at these values of U_{av}/f_nL can be compared directly with the contours of constant v_{rms} /U_{av} of figure 5. At $U_{av}/f_nL = 0.78$, the velocity spectra along the entire streamwise extent of the shear layer shown in figure 6 indicate lack of a well-defined spectral component. On the other hand, at $U_{av}/f_nL = 1.44$, a well-defined spectral peak exists along the entire shear layer, thereby indicating that the enhanced organization and oscillation amplitude of the shear layer at this value of reduced velocity is a global occurrence along the cavity opening. Furthermore, the overall

form of the velocity spectra at U_{av}/f_nL = 1.44 in Figure 6 is close to the form of the corresponding pressure spectrum in Figure 4.

Figure 7 shows contours of constant Reynolds stress $<u'v'>/U_{av}^2$ at the same values of dimensionless velocity U_{av}/f_nL as for the patterns of v_{rms}/U_{av} in Figure 5. These patterns of $<u'v'>/U_{av}^2$ and v_{rms}/U_{av} show the same general trends for increasing U_{av}/f_nL: an increasing value of peak magnitude up to the occurrence of maximum coupling at U_{av}/f_nL = 1.44, followed by a decrease in magnitude for further increases of U_{av}/f_nL. In Figure 7, the peak value of Reynolds Stress at U_{av}/f_nL = 1.44 is more than twice as large as the peak value at U_{av}/f_nL = 0.78, thereby reinforcing the observation that occurrence of strong coupling between the separated shear layer along the cavity opening and the gravity standing wave within the cavity has a large influence on the flow characteristics of the separated shear layer.

The patterns of Reynolds stress shown in Figure 7 indicate that the largest values occur in the separated shear layer along the opening of the cavity. Enhanced Reynolds stress in the separated layer is expected to increase its entrainment demand, that is, the flow towards the layer. More specifically, one anticipates an increase of magnitude of the time-averaged transverse velocity component v towards the separated layer.

Figure 8 shows contours of constant (time-averaged) normalized transverse velocity $<v>/U_{av}$ for the same values of reduced velocity U_{av}/f_nL as in Figure 7. Along the upstream wall of the cavity, the magnitude of $<v>/U_{av}$ is relatively low at U_{av}/f_nL = 0.78, relative to the magnitude at higher values of U_{av}/f_nL where a degree of coupling occurs between the separated shear layer and the gravity standing wave. In fact, the peak magnitude of $<v>/U_{av}$ in these cases is a factor of two larger than the magnitude at U_{av}/f_n-

$_nL$ = 0.78. This enhanced flow out of the cavity towards the separated shear layer must be balanced by a corresponding increase of flow into the cavity, which has its largest values on the vertical wall that forms the downstream side of the cavity. At values of U_{av}/f_nL that exceed U_{av}/f_nL = 0.78, the peak value of $<v>/U_{av}$ is also approximately a factor of two larger than the value at U_{av}/f_nL = 0.78. In essence, the coupling between the separated shear layer and the standing gravity wave within the cavity promotes enhanced flow out of, as well as into, the cavity. This enhancement is accompanied by corresponding enhancement of the Reynolds stress in the separated shear layer.

Figure 9 provides patterns of normalized, time-averaged vorticity $\omega L/U_{av}$, in which ω is the magnitude of vorticity oriented orthogonal to the image (xy) plane.These patterns are of a generally similar form. Comparison of the contour lines at U_{av}/f_nL = 1.44, relative to those at U_{av}/f_nL = 0.78, indicates that the downstream tip of each contour is generally displaced in the upstream direction at the higher values of reduced velocity, relative to the lower value. This observation indicates that the enhanced values of root mean square velocity and Reynolds stress at U_{av}/f_nL = 1.44, which are shown respectively in Figures 5 and 7, promote attenuation of time-averaged magnitude of vorticity along the separated shear layer.

4.2 Phase-Averaged Images

In order to further identify flow structures associated with the gravity standing wave in the cavity, a phase-averaging scheme was implemented. This scheme, which used the pressure transducer in the cavity as a reference, allowed sorting of the instantaneous images at a desired value of phase of the pressure oscillation. This sorting was

implemented for the inflow velocity $U_{av}/f_nL = 1.44$, at which the amplitude of the spectral peak of pressure has its maximum value.

Figure 10 shows images of phase-averaged vorticity $<\omega>_pL/U_{av.}$ At $\Phi = 0°$, the onset of vortex formation is evident as a cluster of elevated vorticity, which is located immediately downstream of the leading corner of the cavity. Subsequent images, at larger values of Φ, show the continued development of the large-scale vortical structure, followed by its eventual impingement upon the corner of the cavity, and deflection of a portion of the vorticity along the impingement wall, into the cavity.

Figure 11 shows contours of constant cross-stream velocity $<v>_p/U_{av.}$ Unlike the aforementioned patterns of vorticity in Figure 10, substantial levels of $<v>_p/U_{av}$ are evident both in the shear layer along the mouth of the cavity and within the cavity, and it is possible to determine the relationship between the transverse velocity fluctuations in the shear layer and those in the cavity. Each pair of positive-negative concentration of vorticity $<v>_p/U_{av}$ in the separated shear layer corresponds to a concentration of vorticity in Figure 10. At $\Phi = 0°$ in Figure 10, representing the onset of vortex formation in the separated layer, a region of high positive vorticity $<\omega>_pL/U_{av}$ extends in a continuous fashion from the layer to well within the cavity. At $\Phi = 80°$, the large concentration of vorticity in the shear layer becomes separated from that within the cavity, and the spatial extent of this separation becomes larger for successively larger values of Φ; simultaneously, the region of large vorticity $<\omega>_pL/U_{av}$ retreats downward within the cavity. But at $\Phi = 200°$, the region of large vorticity $<\omega>_pL/U_{av}$ moves upward towards the separated shear layer until, at $\Phi = 320°$, it is positioned to match the developing vorticity concentration that emerges at $\Phi = 360°$ ($\Phi = 0°$). In essence, the spatial extent

and magnitude of the vertical velocity $\langle v \rangle_p / U_{av}$ within the cavity, oriented towards the separating shear layer, is synchronized with the development of the vorticity concentration in the layer.

5. CONCLUSIONS

The aim of this investigation is to characterize the nature of coupling between: (i) an inherent instability of a shallow, fully turbulent separated shear layer along the opening of a cavity; and (ii) a mode of a gravity standing wave within the cavity. This coupling is expected to influence the structure of the shear layer, as well as the flow within the cavity. A technique of particle image velocimetry is employed in conjunction with pressure measurements in a shallow flow facility. The principal findings are as follows.

Excitation of a gravity standing wave in a shallow water system with a free surface can be effectively attained in presence of a fully turbulent inflow. The frequency of the gravity standing wave is in close agreement with that predicted from theory.

Coupling between the standing wave and the inherent instability frequency of the separated, fully turbulent inflow can lead to a locked-on state. This state is associated with: organized undulations of the free surface; nearly periodic pressure fluctuations within the cavity; and formation of highly organized vortical structures in the separated turbulent layer along the cavity opening. At a sufficiently large inflow velocity, the frequency of the inherent instability of the separated shear layer locks-on to the frequency of the gravity standing wave. Moreover, the amplitude of the spectral peak of the pressure fluctuation attains a maximum value at two different locations: at the impingement corner of the cavity; and well within the cavity. At still larger values of inflow velocity, these

pressure amplitudes decrease, even though the locked-on state of the frequency is maintained. Despite these large variations of amplitude of the spectral peak of the pressure fluctuation over a range of inflow velocity, the spectral peaks remain sharp, that there is, there is no broadening of the spectrum.

The occurrence of the locked-on state of the coupling between the separated shear layer and the gravity standing wave gives rise to substantial increases in the peak magnitudes of Reynolds stress and root mean square velocity fluctuation in the separated shear layer, relative to the pre-locked-on state that occurs at lower values of inflow velocity. Furthermore, time-averaged patterns of the transverse velocity component indicate that the onset of lock-on gives rise to enhanced flow from the cavity towards the separated shear layer in the region immediately downstream of flow separation and, correspondingly, increased flow from the shear layer, towards the cavity in the region of shear layer impingement upon the corner of the cavity. The increased entrainment demands due to increased Reynolds stress in the separated shear layer are the origin of the increase flow towards the shear layer during the locked-on state. In essence, the occurrence of lock-on influences both the magnitude of the turbulence statistics in the separated shear layer and the recirculation flow within the cavity.

Phase-averaged representations of the separated shear layer along the opening of the cavity, during occurrence of the locked-on state, indicate formation of highly ordered, repetitive concentrations of vorticity. The corresponding patterns of phase-averaged transverse velocity indicate large excursions of transverse velocity along the separated shear layer and within the cavity. There is a high correlation between development of the

vortical structure in the separated shear layer along the cavity, and the large magnitude transverse velocity oriented towards the shear layer.

REFERENCES

Chan, F.C., Ghidaoui, M.S. and Kolyshkin, A.A. 2006 “Can the Dynamics of Shallow Wakes be Reproduced from a Single Time-Averaged Profile”, *Physics of Fluids*, Vol. 18, pp. 048105-048105-4.

Chen, F. and Ikeda, S. 1996 "Experimental Study on Horizontal Separation Eddies in Open-Channel Flow with Groynes", *Annual Journal of Hydraulic Engineering – JSCE*, Vol. 40, pp. 777-792.

Chen, D. and Jirka, G.H. 1995 "Experimental Study of Plane Turbulent Wakes in a Shallow Water Layer", *Fluid Dynamics Research*, Vol. 16, No. 11, July, pp. 11-41.

Chen, D. and Jirka, G.H. 1997 "Absolute and Convective Instabilities of Plane Turbulent Wakes in Shallow Water Layer", *Journal of Fluid Mechanics*, Vol. 339, pp. 157-172. [http://jfmwww.damtp.cam.ac.uk/]

Chen, D. and Jirka, G.H. 1998 "Linear Stability Analysis of Turbulent Mixing Layers and Jets in Shallow Water Layers", *Journal of Hydraulic Research*, Vol. 36, No. 5, pp. 815-830.

Chu, V. H. and Babarutsi, S. 1988 "Confinement and Bed-Friction Effects in Shallow Turbulent Mixing Layers", *Journal of Hydraulic Engineering*, ASCE, Vol. 114, No. 10, pp. 1257-1274. [http://scitation.aip.org/hyo/]

Chu, V.H., Wu, J.H. and Khayat. R.E. 1991 "Stability of Transverse Shear Flows in Shallow Open Channels", *Journal of Hydraulic Engineering*, ASCE, Vol. 117, No. 10, pp. 1370-1388. [http://scitation.aip.org/hyo/]

Dracos, T., Geiger, M. and Jirka, G.H. 1992 "Plane Turbulent Jets in a Bounded Fluid Layer", *Journal of Fluid Mechanics*, Vol. 241, pp. 587-614. [http://jfmwww.damtp.cam.ac.uk/]

Ekmekci, A. and Rockwell, D. 2007 "Oscillation of Shallow Flow Past a Cavity: Resonant Coupling with a Gravity Wave", *Journal of Fluids and Structures*, Vol. 23, pp. 809-838.

Giger, M.T., Dracos, T. and Jirka, G.H. 1991 "Entrainment and Mixing in Plane Turbulent Jets in Shallow Water," *Journal of Hydraulic Research*, Vol. 29, pp. 615-641.

Ikeda, S., Yoshike, T., and Sugimoto, T. 1999 "Experimental Study on the Structure of Open Channel Flow with Impermeable Spur Dikes", *Annual Journal of Hydraulic Engineering – JSCE*, Vol. 43, pp. 281-286.

Ingram, G.R. and Chu, V.H. 1987 "Flow around Islands in Rupert Bay: An Investigation of the Bottom Friction Effect," *Journal of Geophysical Research*, Vol. 92(C13), pp. 14,521–14,533.

Jirka, G.H. 1994 "Shallow Jets". In Recent Research Advances in the Fluid Mechanics of Turbulent Jets and Plumes (Ed. P. A. Davies and M. J. V. Neves), Kluwer Academic Publishers, Dordrecht, Netherlands.

Jirka, G.H., Uijttewaal, W.S.J. 2004 *Shallow Flows.* Taylor and Francis Group, London, UK.

Kimura I., Hosoda, T. 1997 "Fundamental Properties of Flows in Open Channels with Dead Zone." *Journal of Hydraulic Engineering,* ASCE, Vol. 123, No. 2, pp. 98-107

Kolyshkin, A.A. and Ghidaoui, M.S. 2003 "Stability Analysis of Shallow Wake Flows", *Journal of Fluid Mechanics*, Vol. 494, pp. 355-377. [http://jfm-www.damtp.cam.ac.uk/]

Kurzke, M., Weitbrecht, W. and Jirka, G.H. 2002 "Laboratory concentration measurements for determination of mass exchange between groin fields and mainstream" IAHR Conference *River Flow* Louvain de la Neuve, Belgium

McCoy, A., Constantinescu, G. and Weber, L.J. 2008 "Numerical Investigation of Flow Hydrodynamics in a Channel with a Series of Groynes", *Journal of Hydraulic Engineering*, ASCE, Vol. 134, No. 2, pp. 157-172.

Nezu, I. and Onitsuka, K. 2002 "PIV Measurements of Side-Cavity Open-Channel Flows – Wando Model in Rivers", *Journal of Visualization*, Vol. 5, No. 1, pp. 77-84.

Rockwell, D., Naudascher, E. 1994 *Flow-Induced Vibrations*. Dover Publications, Inc., New York, USA.

Socolofsky, S.A. and Jirka, G.H. 2004 "Large-Scale Flow Structures and Stability in Shallow Flows", *Journal of Environmental Engineering and Science*, Vol. 3, No. 5, pp. 451-462. [http://www.environmental-expert.com/magazine/nrc/jees/index.htm]

Uijttewaal, W.S.J., Lehmann, D. and van Mazijk, A. 2001 "Exchange Processes between a River and its Groyne Fields: Model Experiments", *Journal of Hydraulic Engineering*, ASCE, Vol. 127, No. 11, pp. 928-936.

Van Prooijen, B.C. and Uijttewaal, W.S.J. 2002 "A Linear Approach for the Evolution of Coherent Structures in Shallow Mixing Layers", *Physics of Fluids*, Vol. 14, No. 12, pp. 4105-4114. [http://pof.aip.org/]

Weitbrecht, V. and Jirka, G.H. 2001 “Flow patterns and exchange processes in dead zones of rivers” IAHR congress, Beijing, China

APPENDIX

Additional figures are provided in this appendix. The information in these figures is not required for an understanding of the research findings provided in the main text. However, these figures do provide complementary results. Figures A2 and A3 represent patterns of phase-averaged velocity fluctuation and Reynolds stress. These patterns were obtained using the same procedure as for the phase-patterns shown in figures 10 and 11 of the main body the text. That is, these phase-averaged statistics were determined within each phase window using the phase sorting scheme described on pages 11 and 17 of the text. Further assessment is required, in order to relate the peak values at each phase to the corresponding time-averaged representations of the same turbulence qualities, which are given in figures 5 and 7 of the main text.

Figure A4 and A5 show variations of frequency of oscillation with inflow velocity at both pressure detection locations, P_a and P_b. All detectable spectral peaks are indicated in these figures. It is evident that both plots are very similar,, but the onset of lock on occurs later within the cavity. Also, nonlinear effects are apparent in the form of frequency components approximately 50% higher than the primary frequency component.

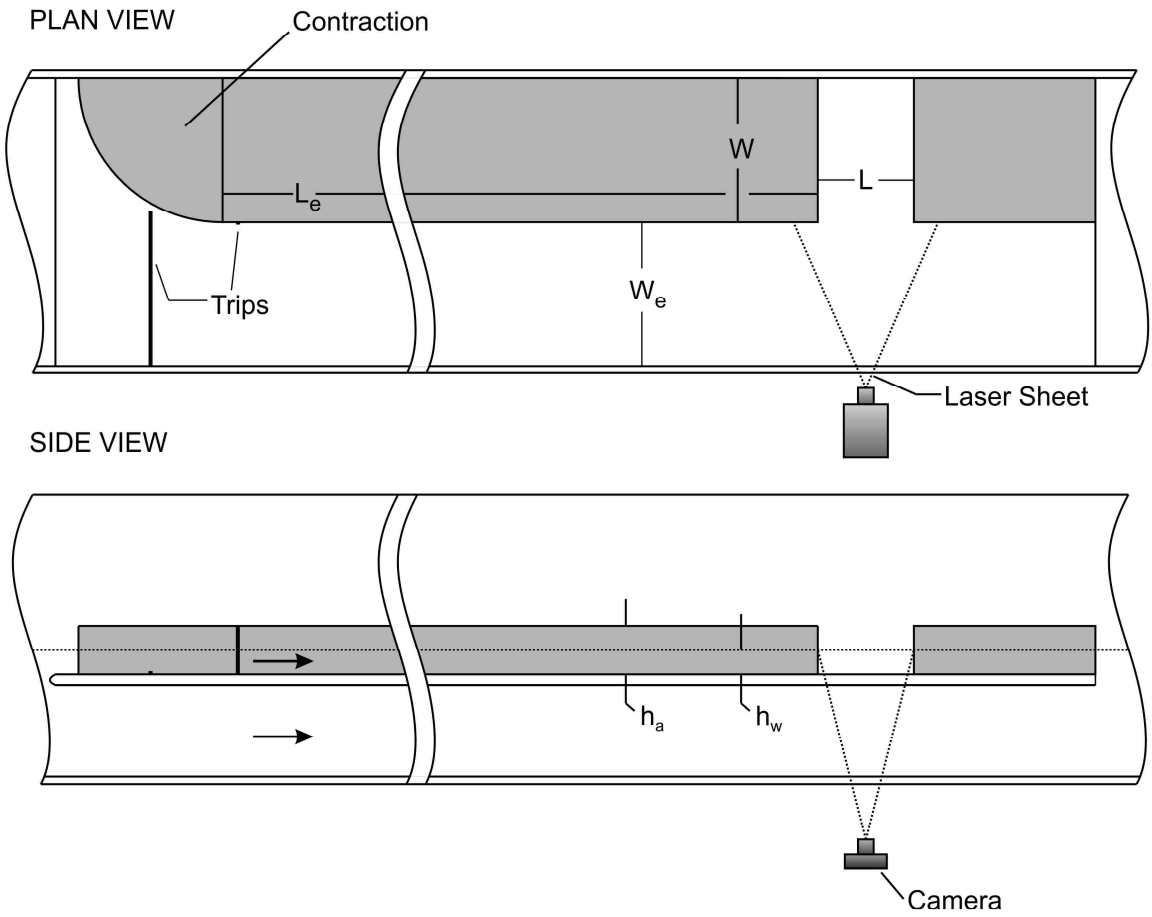

Figure 1a: Schematic of water channel test section and insert for investigation of shallow flow.

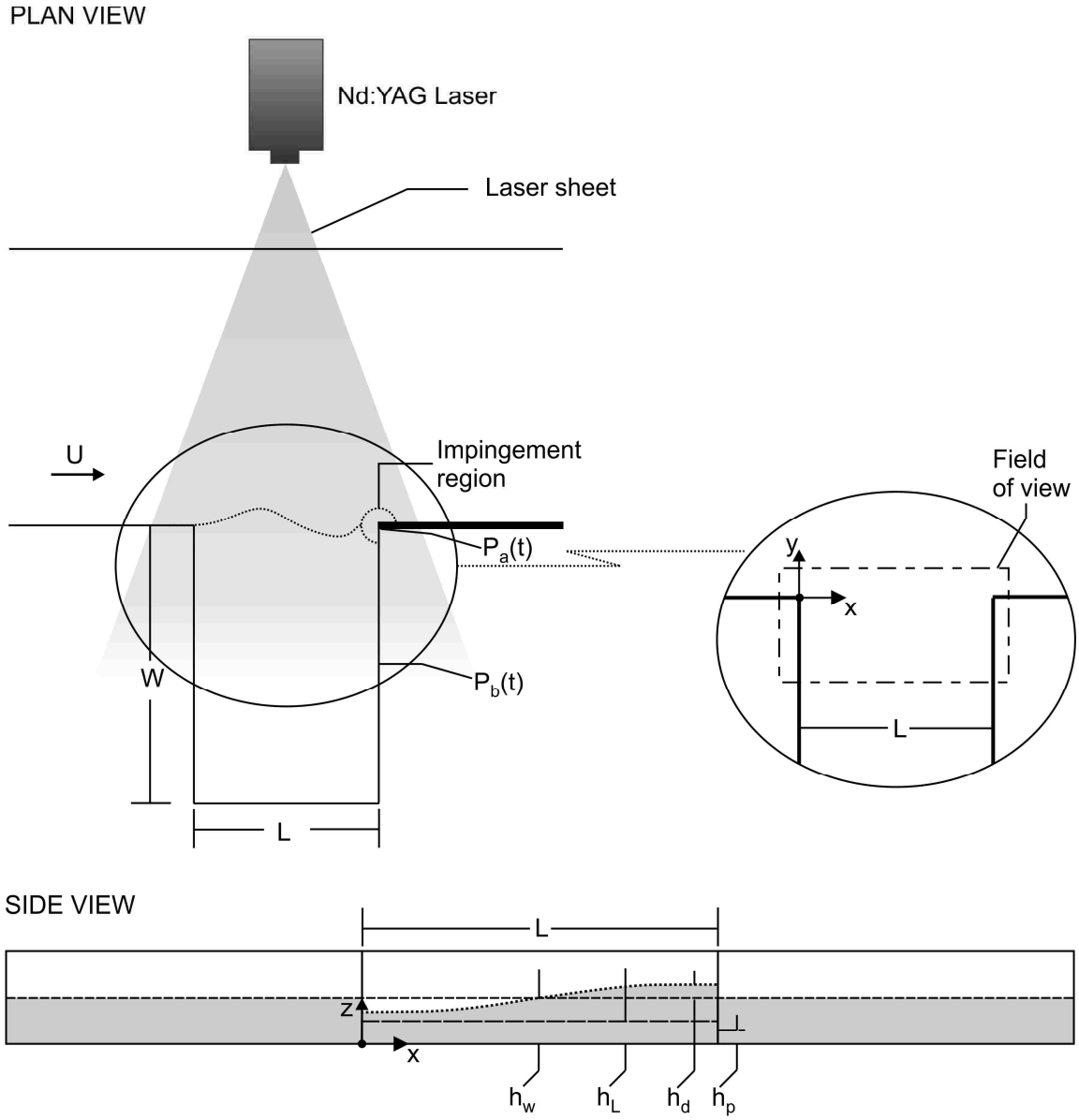

Figure 1b: Schematic of experimental test section including quantitative imaging system, undulating sheer layer along mouth of cavity, and unsteady detection of the surface due to resonant mode of gravity wave within the cavity.

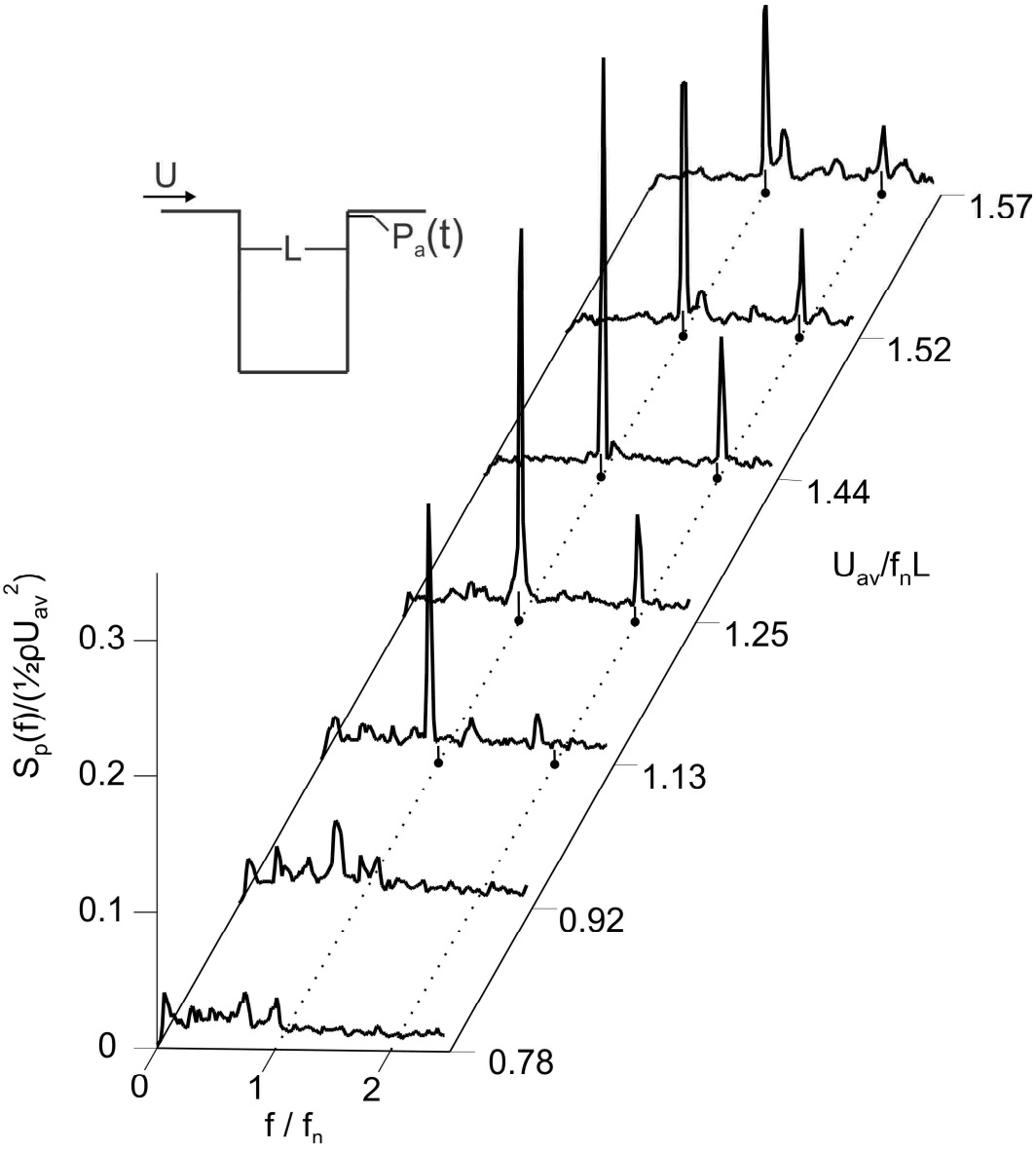

Figure 2: Spectral response of pressure fluctuation at the impingement corner of cavity as a function of dimensionless velocity of inflow.

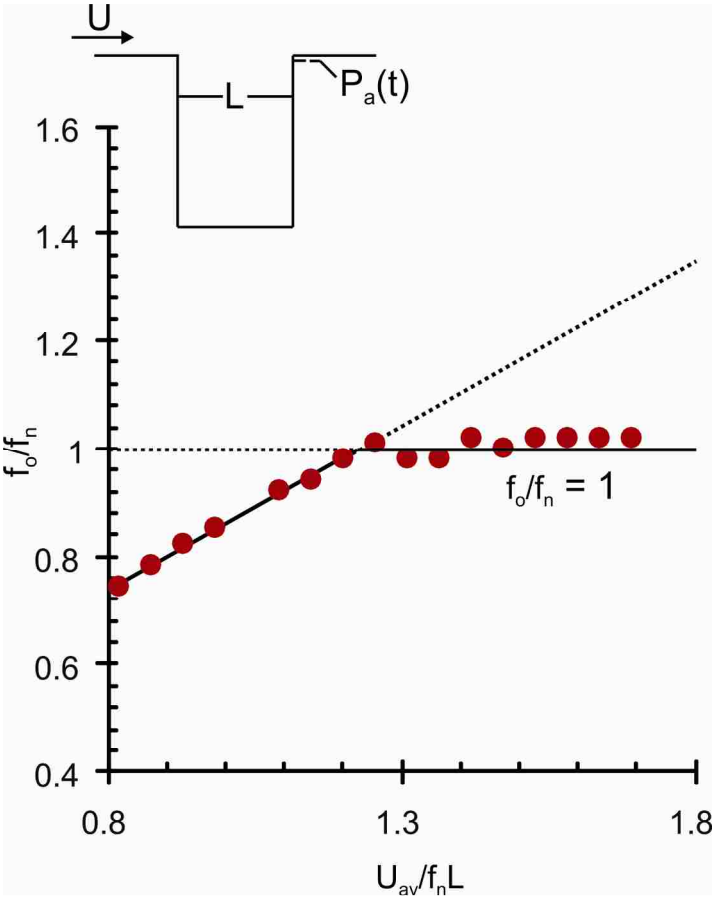

Figure 3: Frequency of peak spectral response of pressure fluctuation at the impingement corner as a function of inflow velocity.

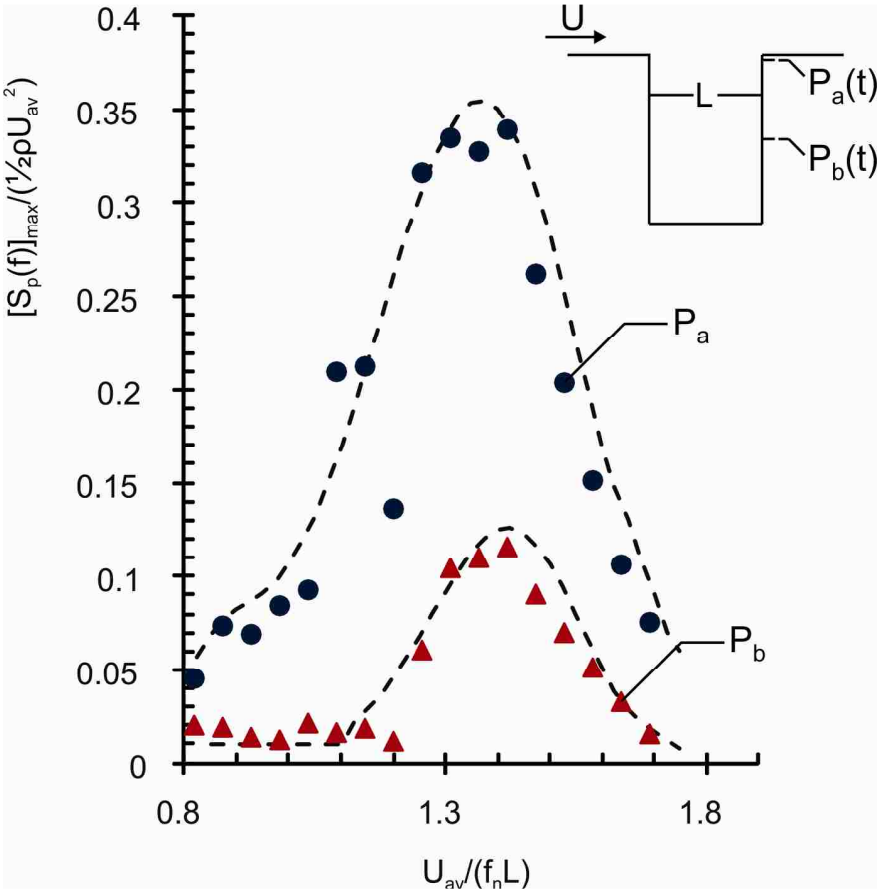

Figure 4: Amplitude of spectral peak of fluctuating pressure at two locations as a function of inflow velocity.

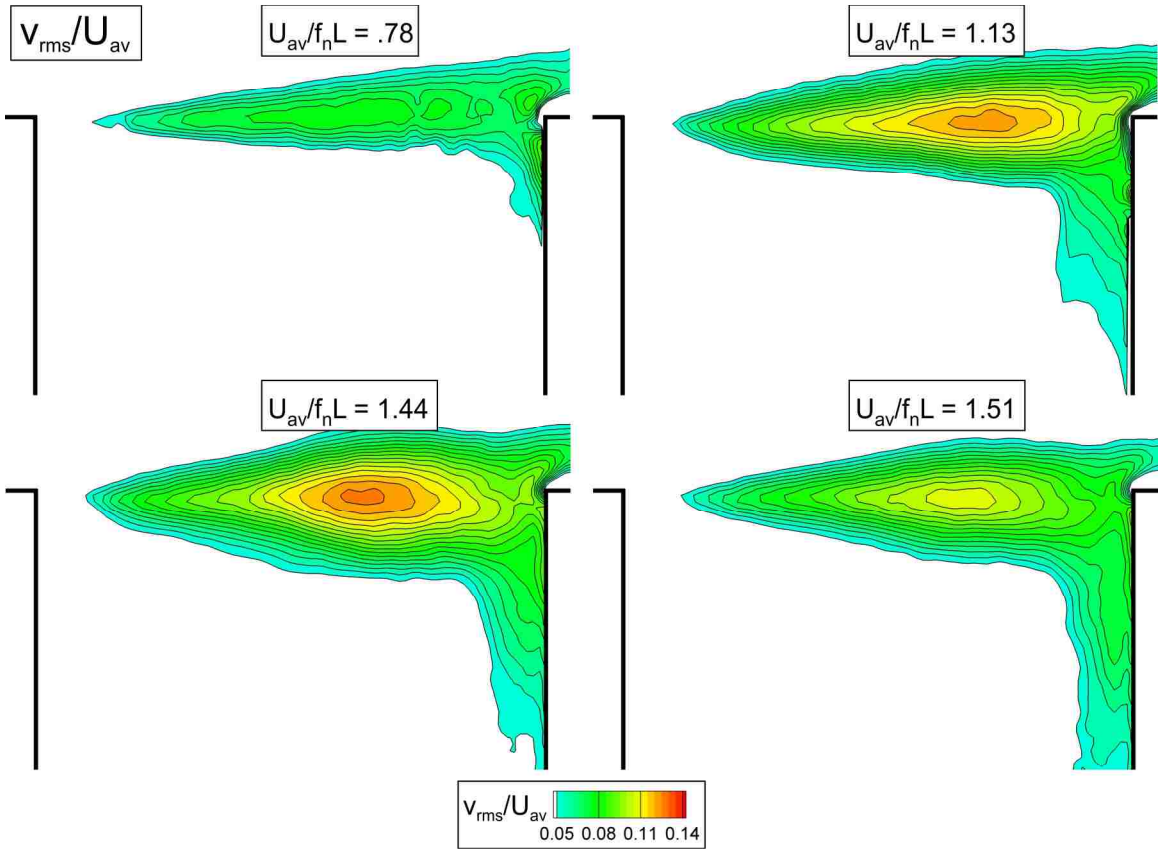

Figure 5: Contours of constant root-mean-square of cross stream velocity as a function of inflow velocity.

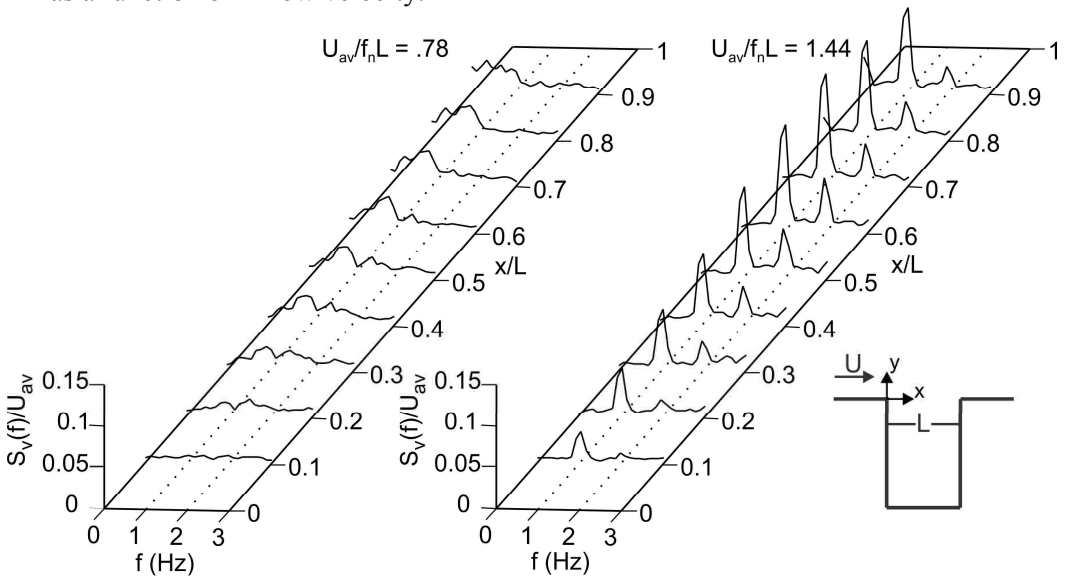

Figure 6: Spectral response of cross-stream velocity fluctuation along the shear layer of a shallow cavity (variable x/L along y/L =0) in absence of gravity-wave coupling (U_{av}/f_nL = 0.78; left image) and with coupling (U_{av}/f_nL = 1.44; right image)

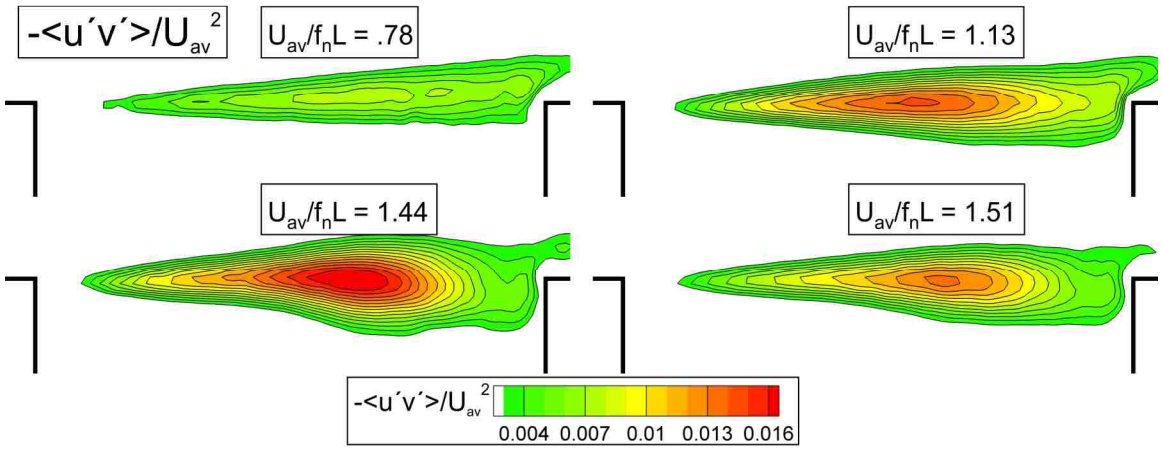

Figure 7: Contours of constant Reynolds Stress as a function of inflow velocity.

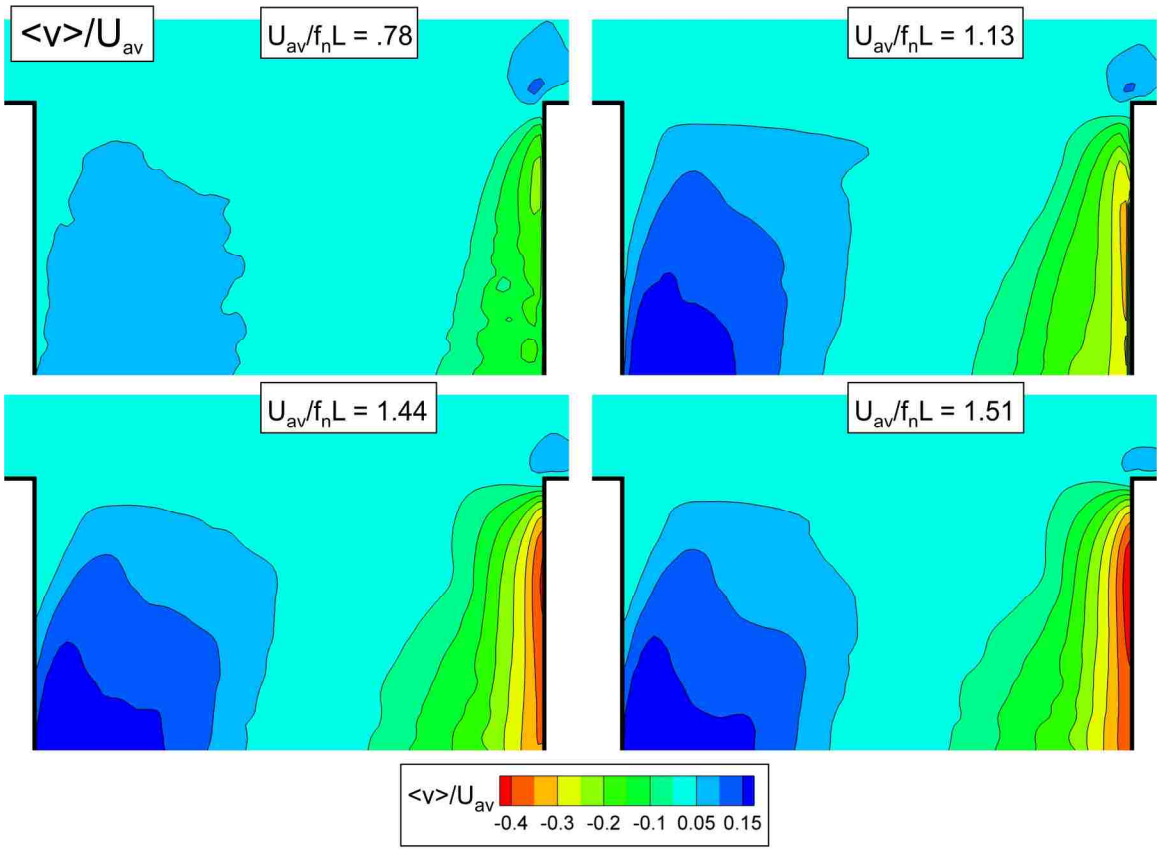

Figure 8: Contours of constant time-averaged cross stream velocity as a function of inflow velocity.

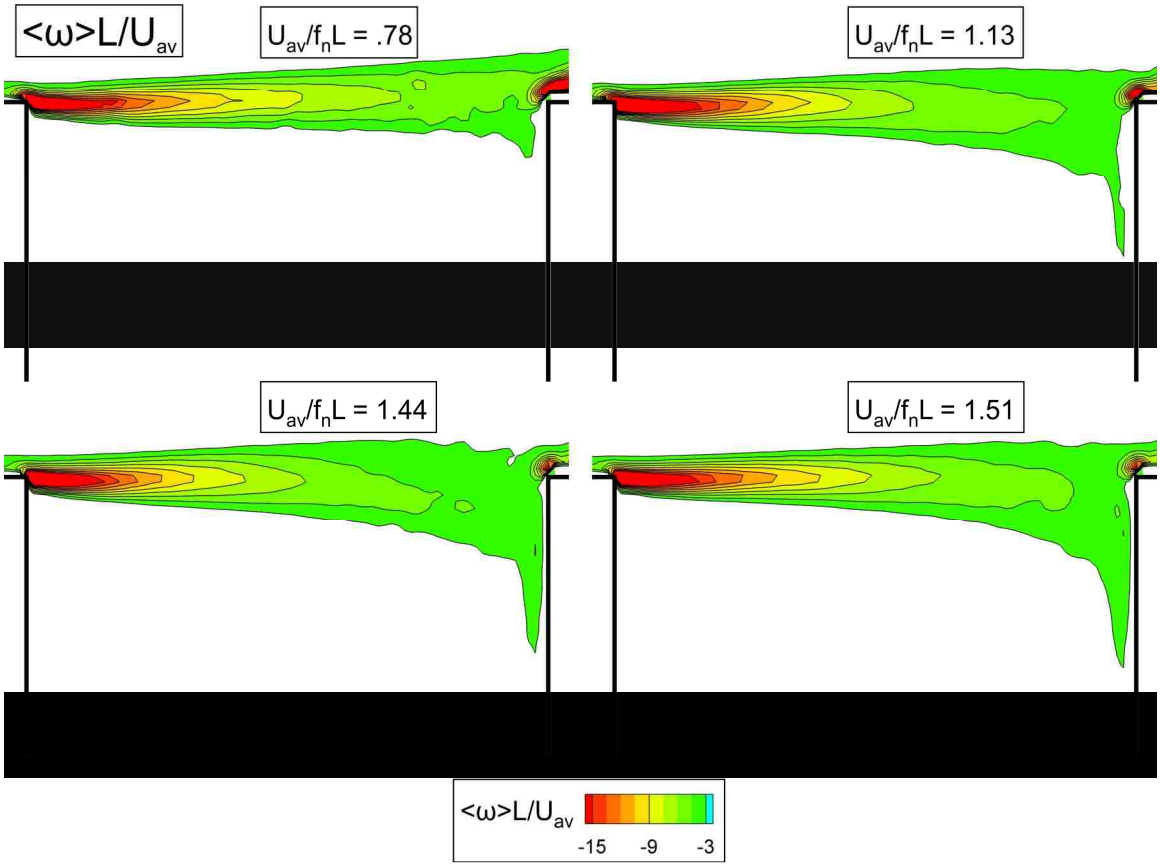

Figure 9: Contours of constant time-averaged vorticity as a function of inflow velocity.

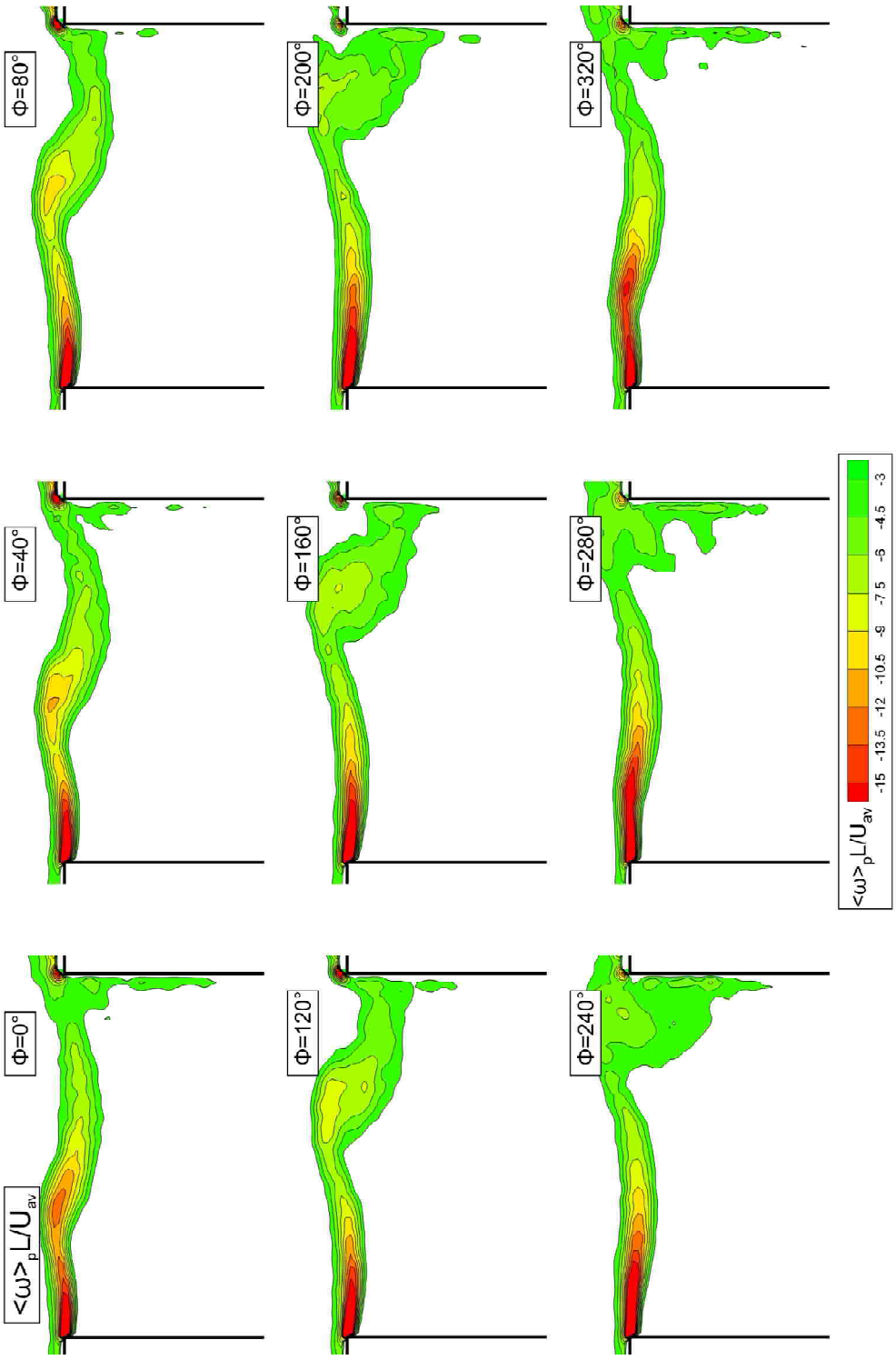

Figure 10: Contours of constant phase-averaged vorticity at 40° intervals for dimensionless velocity $U_{av}/f_nL = 1.44$, corresponding to coupling of shear layer instability along the opening of cavity and a streamwise-oriented gravity wave within the cavity.

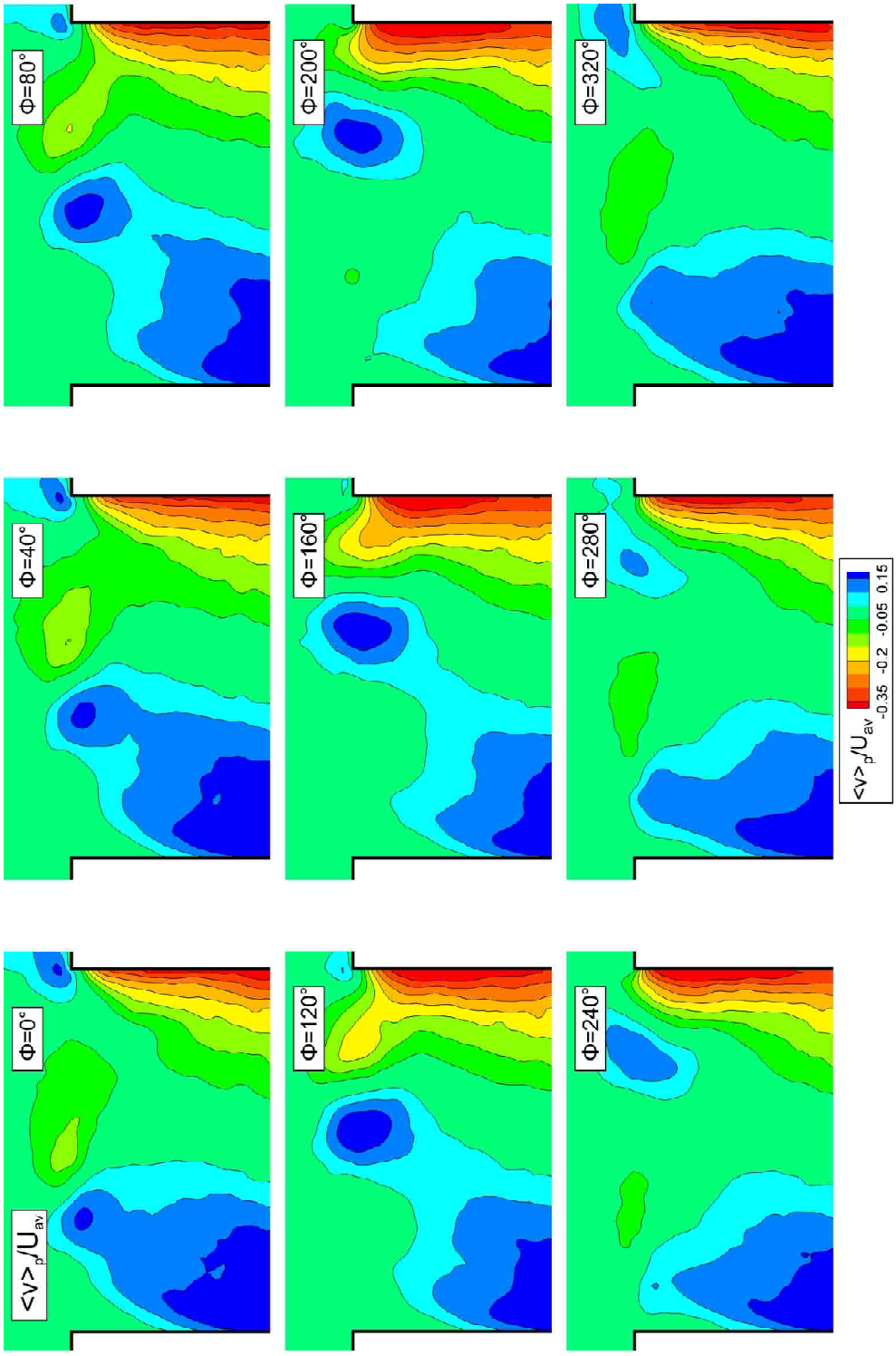

Figure 11: Contours of constant phase-averaged cross-stream velocity at 40° intervals for dimensionless velocity $U/f_nL = 1.44$, corresponding to coupling of shear layer instability along the opening of cavity and a streamwise-oriented gravity wave within the cavity.

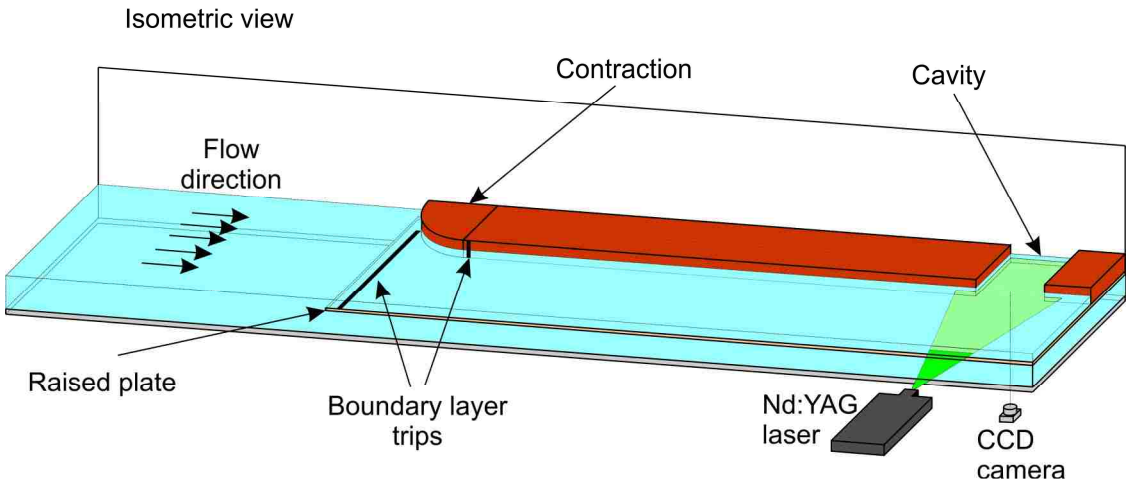

Figure A1: Isometric view of water channel test section and insert

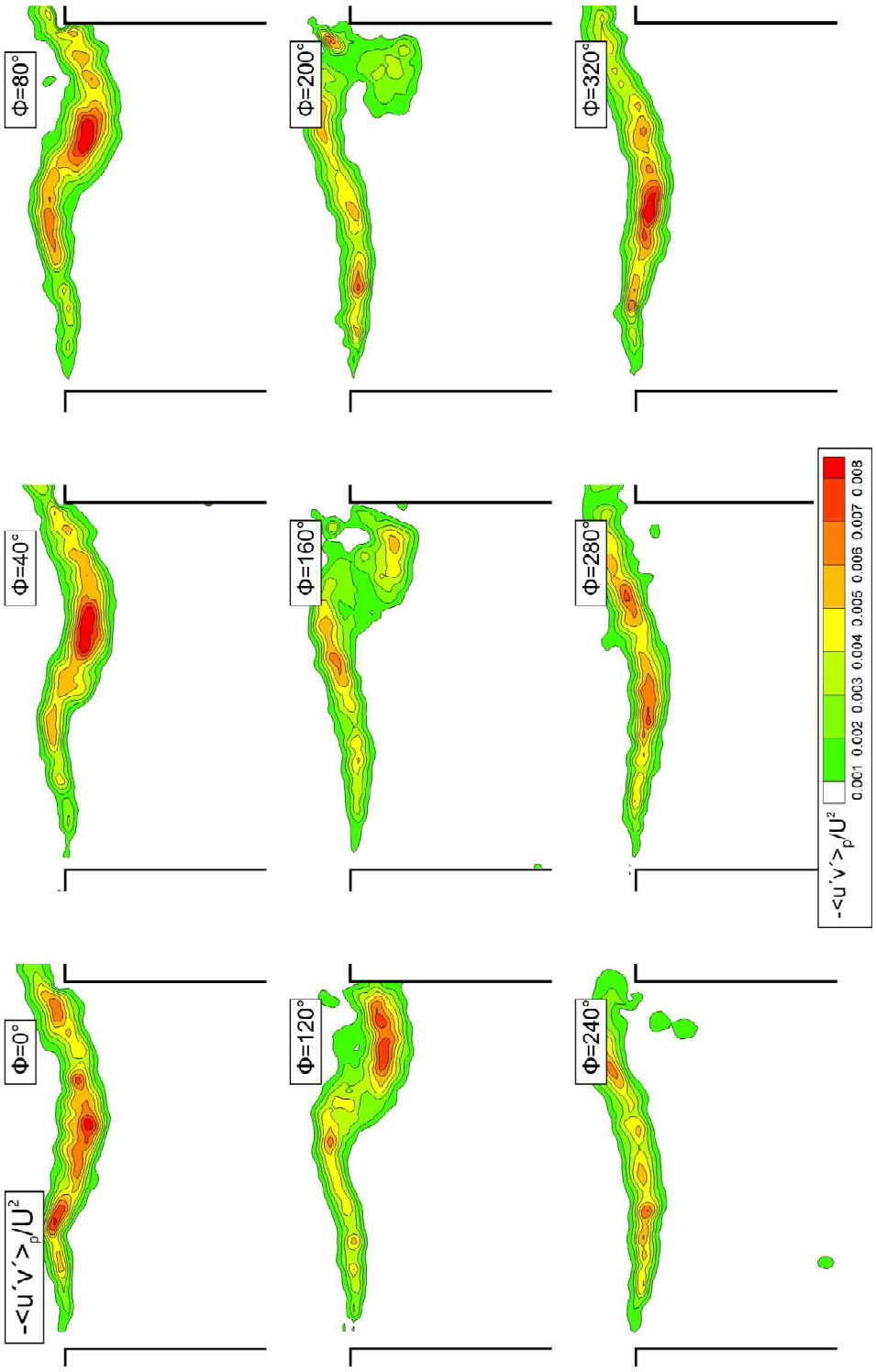

Figure A2: Contours of constant Reynolds Stress at 40° intervals for dimensionless velocity $U/f_nL = 1.44$, corresponding to coupling of shear layer instability along the opening of cavity and a streamwise-oriented gravity wave within the cavity.

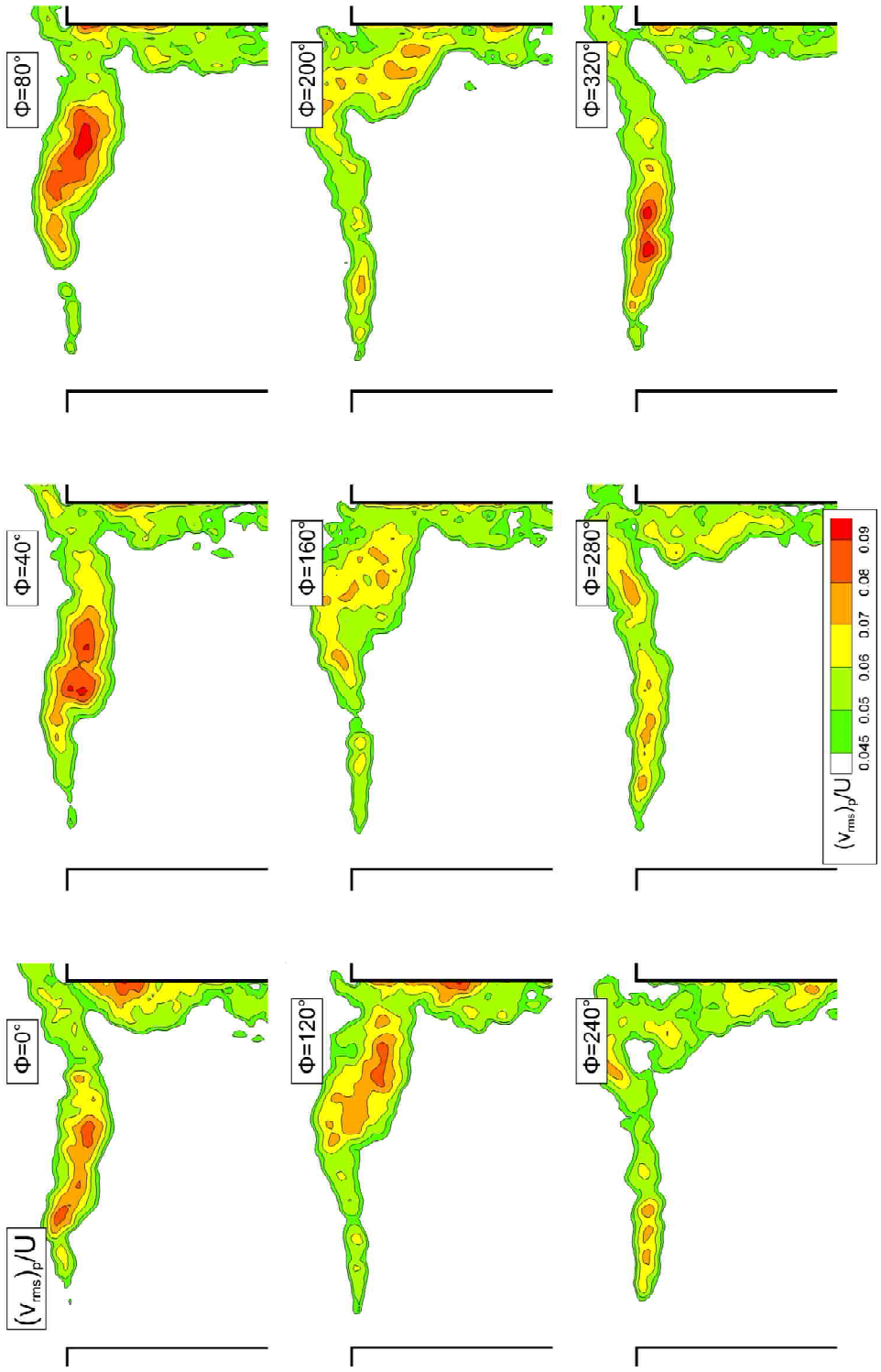

Figure A3: Contours of constant root mean square of cross-stream velocity at 40° intervals for dimensionless velocity $U/f_nL = 1.44$, corresponding to coupling of shear layer instability along the opening of cavity and a streamwise-oriented gravity wave within the cavity.

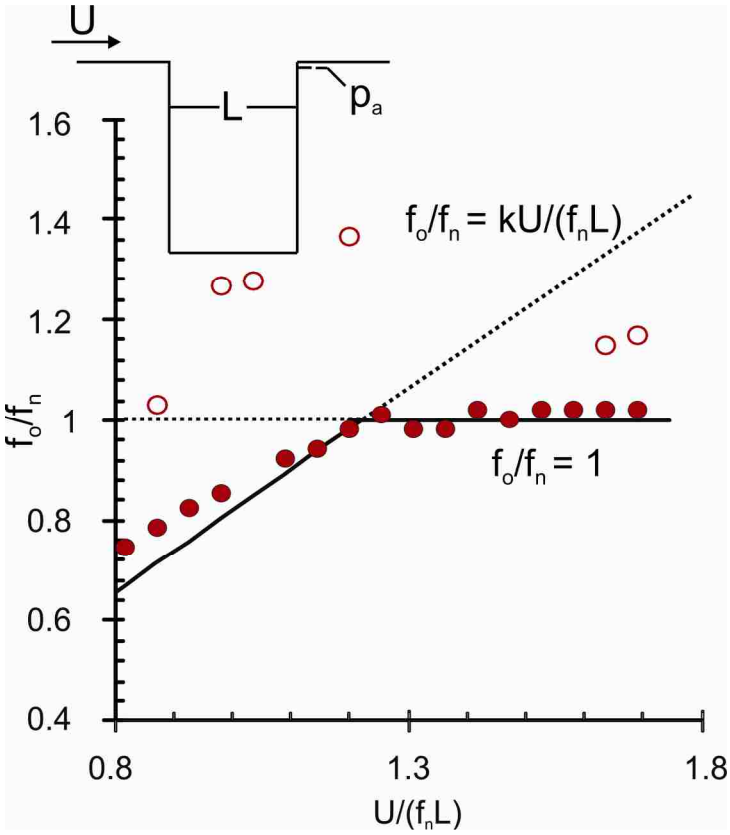

Figure A4: Frequency of peak spectral response of pressure fluctuation at the impingement corner as a function of inflow velocity, including those not representing the primary gravity wave resonance.

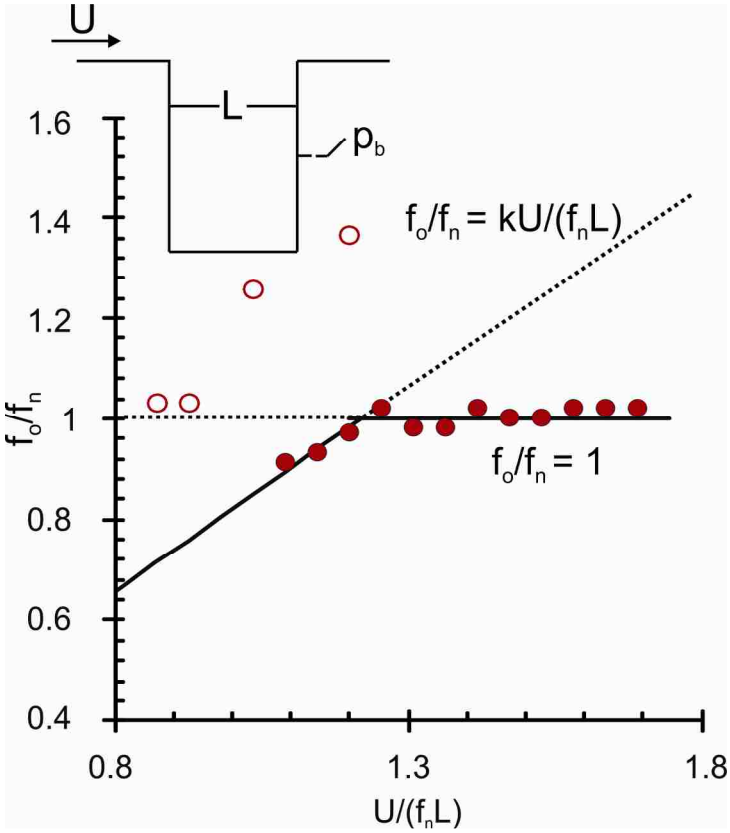

Figure A5: Frequency of peak spectral response of pressure fluctuation inside the cavity as a function of inflow velocity including those not representing the primary gravity wave resonance.

VITA

Maxwell Wolfinger was born in Princeton, New Jersey on April 2, 1987 to Patricia and Raymond Wolfinger. He received a Bachelor of Science degree in Physics with cum laude distinction from Ramapo College of New Jersey in June of 2010. He married his wife, Kate in September of 2011 and now lives with her in Clinton, New Jersey. He was advised for this Master's thesis by Donald Rockwell and plans to continue at Lehigh pursuing a PhD in Mechanical Engineering.